21st Australasian Fluid Mechanics Conference
Adelaide, Australia
10-13 December 2018

On the Evolution of Soot in Laminar Diffusion Flames, Part I: Effects of Oxygen Enhancement in the Coflow Stream

Awais Ashraf[1], Daniel Bartos[1], Matthew Dunn[1], Mariano Sirignano[2], Andrea D'Anna[2], Assaad R. Masri[1]

[1]School of Aerospace, Mechanical and Mechatronic Engineering
The University of Sydney, Sydney, New South Wales 2006, Australia

[2]Dipartimento di Ingegneria Chimica, dei Materiali e della Produzione Industriale,
Universita`degli Studi di Napoli Federico II, Napoli, Italy

Abstract

This study highlights the effects of coflow oxygen concentration on soot and soot precursors in axi-symmetric laminar coflow diffusion flames stabilized on a Yale laminar coflow diffusion burner. Ultraviolet and Infrared range pulsed lasers are utilised to excite soot-precursors and soot particles respectively. Time-resolved laser induced fluorescence (LIF) and laser induced incandescence (LII) are employed to study concentration, size and growth of the particles. The reference flame has jet composition as 60% Ethylene/ 40% Nitrogen, and coflow composition as 21% oxygen/ 79% Nitrogen. In other flames, the jet composition remains the same but oxygen concentration in coflow stream is varied from 19 to 40% leading to a change in the adiabatic temperature, luminosity and flame length. LII signal, a proportional indictive of soot volume fraction, shows a reversal effect with increasing coflow oxygen concentration. With increasing coflow oxygen concentration, LIF signal, a proportional indictive of precursors' concentration, initially increases and then stays stable.

Introduction

Understanding the mechanisms of formation and growth of nanoparticles remains an active area of combustion research considering the importance and complexity of related processes [1]. Carbonaceous nanoparticles are harmful to health [2] and, on the other hand, have applications in different industries [3]. Various techniques have been developed to reduce soot formation and two such techniques are oxygen enhancement, and carbon dioxide dilution.

Oxygen-enhancement influences soot emission in two ways; formation and oxidation. Higher oxygen concentration will lead to a higher flame temperature. On rich side of reaction zone, higher temperature will promote fuel pyrolysis, inception and surface growth. The combined effect on rich side would be increased soot formation. On lean side of reaction zone, higher oxygen and temperature will promote soot oxidation. Therefore, soot emission from an oxygen enhanced flame will be a net result of these competing mechanisms, soot formation and soot oxidation [4].

Although several studies have focused on the effects of oxygen enhancement on soot formation, yet most of the studies have focused on only one parameter, soot volume fraction, to explain the effects of oxygen-enhancement [5, 6].

A study investigated the effects of oxygen-enhancement on soot formation in biodiesel flames [7]. As per results of this study, soot volume fraction increases with oxygen enhancement up to a certain point (threshold oxygen concertation), then soot volume fraction decreases with further oxygen enhancement. Another study focused on effects of oxygen index (21 to 37 %) on soot production in laminar diffusion co-flow propane flames [8]. As per results, soot volume fraction enhanced with oxygen index up to 29% of oxygen. Heat flux also increased with oxygen index.

Effects of oxygen addition in fuel stream on soot formation in methane, propane and n-butane flames were compared [9]. The study found that oxygen enhancement suppressed soot in methane flame due to reduction in acetylene concentration. However, soot formation increased with oxygen in propane and n-butane flames. Another study investigated effects of oxygen enhancement (21 to 100%) in methane laminar coflow diffusion flames [10]. With oxygen-enhancement, flame brightness, temperature and radiative heat flux increase. Injection of pure oxygen in the oxidizing stream causes thermal NO_x as temperature approaches approximately 2900K.

Several studies [11, 12] have employed in-situ laser diagnostic techniques, such as, laser induced incandescence (LII) and laser induced fluorescence (LIF). LII is a reliable and efficient technique to track mature soot particles. LII has applications from laboratory scale flames to practical combustion systems. LIF technique is used to study polycyclic aromatic hydrocarbons (PAHs) and nanoparticles. With appropriate spectral filtering, difference classes of PAHs and nanoparticles can be selectively excited and analysed [13].

This study classifies combustion formed nanoparticles in terms of their spectral properties. Structures with ability to incandesce and absorb in infrared are referred as soot. Nominal diameter of such structures ranges from 10 to 100 nm. Structures with ability to fluoresce and absorb ultraviolet light are called nanostructures. Diameter of such structures can be up to 20 nm. The number density of nanostructures, when compared to that of soot, is almost ten times higher but their mass contribution is negligible [12].

This study focuses on the effects of oxygen-enhancement (19 to 40%) in co-flow stream on soot and soot-precursors for axisymmetric ethylene laminar coflow diffusion flames. Ultraviolet and infrared laser sources are used to excite flame particles. Time resolved LII and LIF techniques are employed to analyse emissions from the excited particles.

Experimental setup

Burner and flames

An axisymmetric laminar Yale burner adopted by the International Sooting Flame Workshop (ISF) is used. The burner has a fuel tube and coflow honeycomb. The fuel tube is a 4mm ID 0.038 mm wall thickness, surrounded by 75/4.76 mm OD/ID concentric co-flow honeycomb duct. Eight flames with the same jet but different coflow composition are studied, table 1. The jet composition is 60% Ethylene/ 40% nitrogen. Jet and coflow velocities are 35 cm/s in all cases.

Laser sources

Up to some extent, it is possible to selectively excite and observe the emitted spectrum of a specific class of nanoparticles. It is carried out by predefining the wavelength and energy of a laser source, and by applying spectral filtering to the emitted spectrum [13]. For example, nanostructures (up to 20 nm) can be excited by 4th harmonic (266 nm) or 5th harmonic (213 nm). Use of 5th harmonic would include relative higher contribution from PAHs in the emitted spectrum. As this experiment is focusing on soot precursors, use of 4th harmonic is preferred [11, 12]. Similarly, it is possible to have soot particles emit incandescence either by using fundamental harmonic (1064 nm) or second harmonic (532 nm). However, use of second harmonic (532 nm) would add contributions from C_2 and C_3 bands in the emitted spectrum. As this experiment is focusing on soot particles, use of fundamental harmonic is preferred.

Flame	Chemical Composition		Flame length (mm)	Soot starting HAB (mm)	Simulated adiabatic temp (K)
	Coflow stream	Jet/ fuel stream			
1	19% O_2 / 81% N_2	60% C_2H_4/ 40% N_2	60	31	2229.6
2	21% O_2 / 79% N_2	60% C_2H_4/ 40% N_2	53	28	2325.3
3	24% O_2 / 76% N_2	60% C_2H_4/ 40% N_2	44	23	2440.6
4	27% O_2 / 73% N_2	60% C_2H_4/ 40% N_2	38	20	2531.9
5	30% O_2 / 70% N_2	60% C_2H_4/ 40% N_2	32	18	2604.2
6	33% O_2 / 67% N_2	60% C_2H_4/ 40% N_2	29	16	2664.7
7	36% O_2 / 64% N_2	60% C_2H_4/ 40% N_2	25	15	2715.8
8	40% O_2 / 60% N_2	60% C_2H_4/ 40% N_2	22	13	2772.8

Table 1: Chemical composition, length, soot starting height and adiabatic flame temperature of different flames are mentioned. The adiabatic temperature is simulated using CHEMKIN.

Two laser sources were used is this study. 4th harmonic of a mode-locked Nd:YAG Ekspla laser (266 nm, 80 ps pulse width) was used to target soot precursors. Its probe diameter was 250 µm resulting in a fluence of 0.57 mJ/cm^2. The fundamental harmonic of a Spectra-Physics Quanta-Ray Pro-350 laser (1064 nm, 8 ns pulse width) was used to excite nanoparticles. Its probe diameter was 450 µm resulting in a fluence of 1.15 mJ/cm^2. 1064 nm laser was delayed by 900 ns from 266 nm pulse to allow the same volume to be probed with both lasers.

Data acquisition and processing

Data acquisition system consisted of four photomultiplier tubes (PMTs), a spectrometer and an oscilloscope. Upon irradiance, excited particles emitted radiation spectrum which was focused on the grating slit of a spectrometer which resolved the incoming radiation spectrum into the component wavelength bands. PMTs collected the component wavelength bands in the time domain. At a later stage, the temporal response was analysed to study the formation, evolution and destruction of the excited particles. PMTs collected the response in narrow wavelength bandwidths such as PMT1 (266 ± 15 nm), PMT2 (350 ± 15 nm), PMT3 (445 ± 15 nm) and PMT4 (575 ± 15 nm). These wavelength bands were chosen very carefully to obtain important segments of the emitted spectrums. PMT1, PMT2, PMT3, and PMT4 recorded scattering, UV LIF, visible LIF, and LII signals respectively.

Signals from the four PMTs were recorded using a Tektronix oscilloscope (25 Giga-sample/s, 4 GHz bandwidth). At each measurement location, 500 instantaneous acquisitions were captured. An integrated signal can represent the overall response from the excited particles. The magnitude of the integrated signal is related to the volume fraction of particles being probed. Peak of signal is related to mass concentration of excited species. Ratio of UV LIF to visible LIF along HAB is an indicative of structural changes. Decay of temporal response is an indicative of size.

Results

In this section, effects of oxygen enhancement on soot volume fraction, precursor concentration, and size of precursors are discussed.

Oxygen enhancement effects on soot volume fraction

IR range (1064 nm) laser induces incandescence spectrum from soot particles. The LII spectrum is collected in temporal domain at four distinct wavelength bins (266±15, 350±15, 445±15, 575±15 nm) using photomultiplier tubes. LII signal collected at @ 575 nm is proportional to SVF.

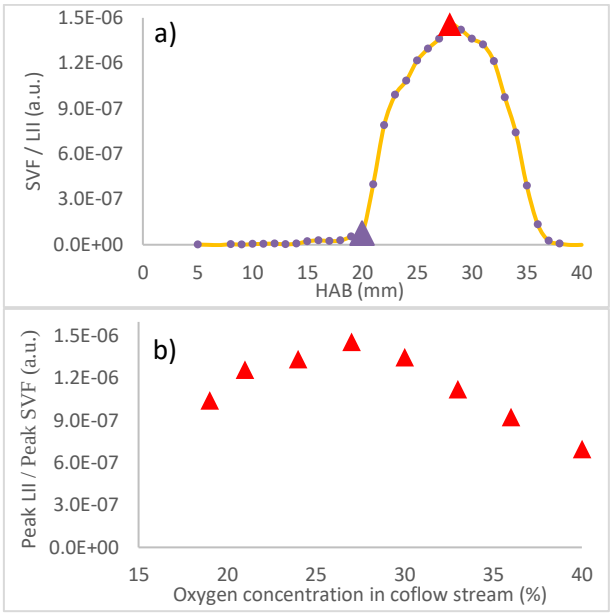

Figure 1: LII / Soot volume fraction along centreline is presented here. 1(a) shows soot volume fraction along centreline of flame 4 (27% O_2). 1(b) shows peak soot volume fraction of all flames w.r.t. coflow oxygen

Figure 1(a) shows integrated LII signal collected at 575nm at different height above burner along the centreline of flame 4 (27% oxygen). The plot can be divided into two regions; a non-sooting region (HAB up to 20mm) and a sooting region (HAB > 20mm). Both regions are separated by a purple triangle. In sooting region, LII signal increases with HAB until it reaches the peak at HAB=30mm. LII peak is marked by a red triangle in figure 1(a). After the peak LII, oxidation region starts where LII signal gradually reduces to negligible values.

Initially, peak SVF increases until coflow oxygen concertation is 27% (threshold oxygen concentration), after which peak SVF starts decreasing with increasing coflow oxygen. The downward trend continues till coflow oxygen concentration is 40%. Figure 1(b) shows peak SVF of all flames w.r.t. coflow oxygen.

This soot reversal trend is in-line with findings of Wang [6] who studied ethylene coflow flames and observed soot reversal effect with respect to oxygen concentration in fuel stream. Wilson [7] also found soot reversal behaviour while investigating effects of coflow oxygen enhancement in biodiesel flames.

Oxygen enhancement effects on concentration of soot precursors

UV range (266 nm) laser induces a fluorescence spectrum from nanostructures. The LIF spectrum is collected in the temporal domain at four distinct wavelength bins (266±15, 350±15, 445±15, 575±15 nm) using photomultiplier tubes. Figure 2 (a) shows peak LIF signal collected at 350 nm for flame 4 (27% oxygen). Peak LIF signal is related to the concentration of excited nanoparticles. Plot in figure 2(a) shows two peaks. Initially, LIF signal increases with HAB until first peak is reached, after which LIF signal decreases for a while followed by an upward trend. First and second peaks are marked by green and blue triangles respectively.

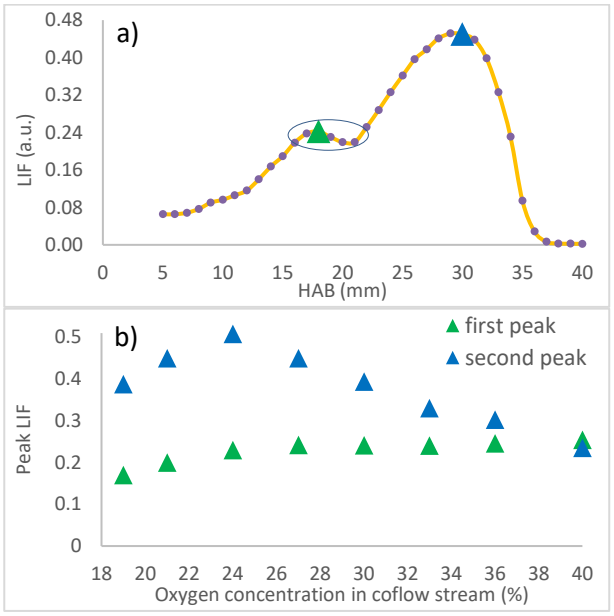

Figure 2: LIF signal along centreline of is presented here. 2a shows LIF signal along centreline of flame 4 (27% O_2). 2b shows first and second LIF peaks for all flames w.r.t. coflow oxygen

Moving away from the burner along the centreline, flame temperature increases which leads to a higher reaction rate, and increased concentration of nanoparticles. Therefore, LIF signal increases. However, just before the onset of soot, LIF drops slightly and rises again. A valley (enclosed by a blue ellipse in figure 2(a)) is called grey region. A possible explanation is transformation of nanoparticles into soot via an intermediate stage where nanoparticles become rigid/ graphitic leading to a lower quantum yield (LIF signal) in that region. Moreover, scattering signal keep on increasing in grey region, figure 3a. LIF signal in first hump may consist of contributions from PAHs, nanoparticles, and C_2 and C_3 bands. However, contribution from nanoparticles is much higher. Therefore, peak of first hump can be related to contribution from nanoparticles.

Second peak is occurring in sooting region. Nanoparticles can co-exist with larger soot particles, and a UV laser (266 nm) can excite both nanoparticles and soot. Moreover, a UV laser with 0.6 mj/pulse can sublimate soot particles which can result C_2 and C_3 interferences. Therefore, second peak of LIF may be a combination of fluorescence, incandescence and contribution from C_2 and C_3 emissions. As nanoparticles are growing with HAB, concentration of small nanoparticles might be reducing in grey region. Moreover, photomultiplier tubes have been placed in such spectral range which would minimize interference from C_2 and C_3 bands. Although second hump trends with LII profile yet spectral positioning of PMT2 (350nm) would receive very low contribution from incandescence spectrum. Therefore, major contributions in second peak of LIF may be from graphitic nanoparticles.

Figure 2(b) shows first and second peaks of LIF for different flames w.r.t. coflow oxygen. Nanoparticle concentration (first peak) increases with coflow oxygen until 27% (threshold concentration) after which the concentration does not change significantly. The second peak increases with coflow oxygen concentration until 24%, after which it decreases with increasing coflow oxygen.

Scattering signal

266nm laser induces a fluorescence spectrum from nanoparticles. The LIF spectrum is collected in temporal domain at four distinct wavelength bins (266±15, 350±15, 445±15, 575±15 nm) using photomultiplier tubes.

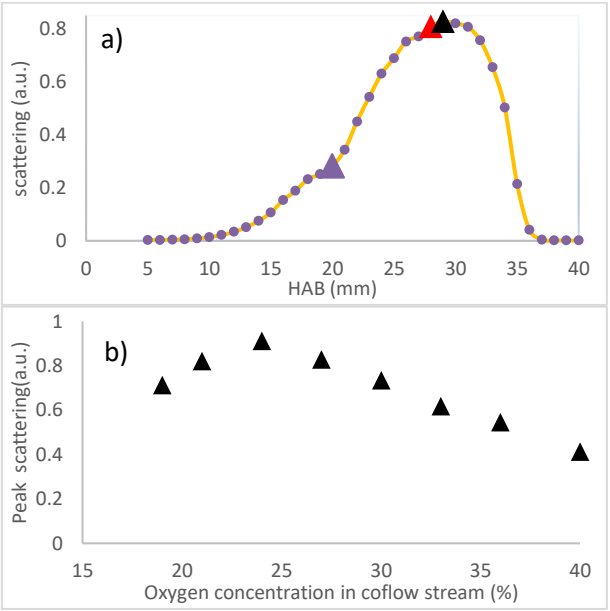

Figure 3: Scattering signal along centreline is presented here. 4a shows scattering signal along centreline of flame 4 (27% O_2). 4b shows peak scattering of all flames w.r.t. coflow oxygen

Figure 3(a) shows peak LIF signal collected at 266nm (Scattering signal) for flame 4 (27% oxygen). Presence of scattering signal in non-sooting region (HAB < 21) indicates that structures other than soot may also contribute towards scattering signal. Fluorescing nanoparticles with 2-20 nm size may be present in this region [14]. Scattering peak is marked by a black triangle. Figure 3(b) shows peak scattering signal of all flames w.r.t. coflow oxygen. Peak scattering increases with coflow oxygen until 24% followed by a downward trend.

With oxygen-enhancement, flame length reduces and so does the residence time of nanoparticles in pyrolytic region. For growth, nanoparticles need to stay for a in pyrolytic region. As with oxygen-enhancement, pyrolytic region is shrinking and oxidation is becoming stronger, growth of nanoparticles is suppressing leading to lower concentration of graphitic/rigid nanoparticles. Therefore, scattering peak is reducing with increasing coflow oxygen.

Discussion

Overall soot formation is a trade-off between fuel pyrolysis rate, resulting from higher flame temperature, and the oxidation

rate of soot within a flame. Higher oxygen concentration results in higher flame temperature which promotes soot inception and nucleation, consequently soot formation is promoted. On the other hand, higher oxygen presence will promote oxidation of soot particles as well. Moreover, flame length (residence time in pyrolytic region) decreases when oxygen increases. To transform into more graphitic /rigid particles, precursors require to stay in the reaction zone. Lower residence time would reduce concentration of rigid/graphitic particles. Before threshold concentration, higher pyrolysis rate results in higher SVF. Beyond threshold concentration, oxidation rate and reduced residence time take over which lead to lower SVF.

Similarly, there is a limit up to which precursor concentration can increase with oxygen. After threshold concentration, further addition of oxygen does not increase precursor concentration due to shrinking pyrolysis region and higher oxidation rate. Interestingly, second peak of LIF shows a reversal effect just like SVF, figure 1(b) and 2(b). This might suggest second peak receives a significant contribution from soot emissions. But spectral position of PMT2 would not support this.

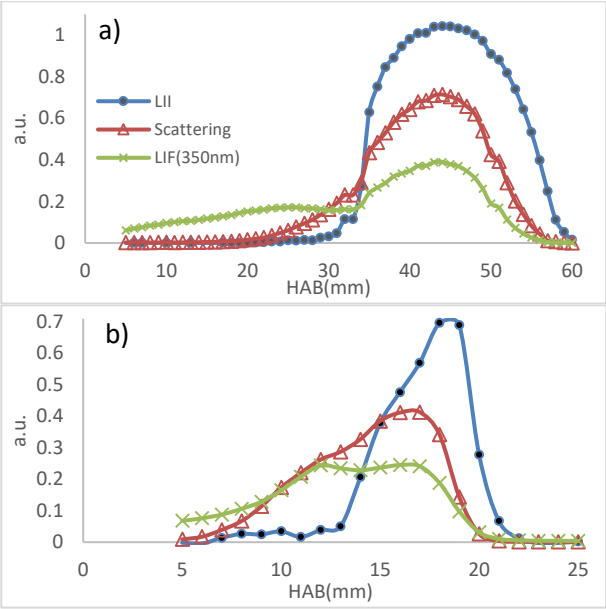

Figure 4: LII, LIF and scattering signals along centreline are presented here. 4a shows signals along centreline of flame 1 (19% O_2). 4b shows signals along centreline of flame 8 (40% O_2)

Figures 2(b) and 3(b) show that scattering peak trends well with second peak of LIF. For all flames, complete profile of scattering and second hump of LIF trend well. Up to threshold coflow oxygen concentration (27%), scattering signal trends well with both LII and second hump of LIF. For example, LII, second hump of LIF and scattering signal trend well for flame 1 (19% oxygen), shown in figure 4(a). For oxygen beyond threshold level, scattering signal trends with second hump of LIF only. For example, second hump of LIF and scattering signal trend well for flame 7 (O_2 as 36%), shown in figure 4(b). Despite LII continues to rise, both scattering and LIF are dropping. Presence of scattering in non-sooting region and its preferential trend with second peak of LIF may indicate that scattering is primarily driven by contribution from rigid/ graphitic nanoparticles.

Conclusion

Effects of oxygen enhancement in coflow stream on soot and soot precursors have been studied using time resolved laser induced emissions. Laser induced incandescence signal is directly proportional to SVF. LII shows a reversal effect with increasing coflow oxygen. Initially LII increases with coflow oxygen. After threshold coflow oxygen level (27% by volume), LII decreases with coflow oxygen. Concentration of precursors increases with oxygen until threshold oxygen level, after which it stays almost unchanged. Presence of scattering signal in non-sooting region indicates that soot is not the only scatterer.

Acknowledgement

This research has been supported by the Australian Research Council.

References

1. D'Anna, A., *Combustion-formed nanoparticles.* Proceedings of the Combustion Institute, 2009. **32**(1): p. 593-613.
2. Chen, R., et al., *Beyond PM2.5: The role of ultrafine particles on adverse health effects of air pollution.* Biochim Biophys Acta, 2016. **1860**(12): p. 2844-55.
3. Mansurov, Z.A., *Soot Formation in Combustion Processes (Review).* Combustion, Explosion, and Shock Waves, 2005. **41**(6): p. 727-744.
4. Oh, K.C., *The effect of oxugen and carbon Dioxide concentration on soot formation in Nonpremixed flames using time resolved LII technique.* Journal of Mechanical Science and Technology, 2005. **19**(11): p. 2068-2076.
5. Wang, L., et al., *A Study of the Influence of Oxygen Index on Soot, Radiation, and Emission Characteristics of Turbulent Jet Flames.* Combustion Science and Technology, 2002. **174**(8): p. 45-72.
6. Wang, Q., et al., *Experimental assessment of the sudden-reversal of the oxygen dilution effect on soot production in coflow ethylene flames.* Combustion and Flame, 2017. **183**: p. 242-252.
7. Merchan-Merchan, W., S. McCollam, and J.F.C. Pugliese, *Soot formation in diffusion oxygen-enhanced biodiesel flames.* Fuel, 2015. **156**: p. 129-141.
8. Henríquez, R., et al., *The Oxygen Index on Soot Production in Propane Diffusion Flames.* Combustion Science and Technology, 2014. **186**(4-5): p. 504-517.
9. Gulder, O., *Effects of Oxygen on Soot Formation in Methane, Propane.* Combustion and Flame, 1995. **101**: p. 302-310.
10. Cheng, Z., et al., *Oxygen-Enhanced High Temperature Laminar Coflow Flames.* 2004.
11. Bartos, D., et al., *Tracking the evolution of soot particles and precursors in turbulent flames using laser-induced emission.* Proceedings of the Combustion Institute, 2017. **36**(2): p. 1869-1876.
12. Sirignano, M., et al., *Detection of nanostructures and soot in laminar premixed flames.* Combustion and Flame, 2017. **176**: p. 299-308.
13. Bejaoui, S., et al., *Laser induced fluorescence spectroscopy of aromatic species produced in atmospheric sooting flames using UV and visible excitation wavelengths.* Combustion and Flame, 2014. **161**(10): p. 2479-2491.
14. Commodo, M., et al., *Size Measurements of Fluorescent Carbon Nanoparticles in a Coflowing Laminar Diffusion Flame by Time-Resolved Fluorescence Anisotropy.* Combustion Science and Technology, 2012. **184**(7-8): p. 916-928.